ELSEVIER

Journal of Nuclear Materials 266–269 (1999) 804–808

journal of nuclear materials

B2-Eirene modelling of the density limit on ASDEX-Upgrade

D.P. Coster *, K. Borrass, R. Schneider, ASDEX-UpgradeTeam

Max-Planck Institut für Plasmaphysik, Boltzmann St. 2, 85748 Garching, Germany

Abstract

The B2-Eirene code package was used to investigate the density limit in ASDEX-Upgrade, both in the old, open divertor configuration and the new, more closed configuration. A combination of time-dependent (directly simulating the experimental scenario of raising the plasma density with an external gas puff) and time-independent runs for discrete densities were performed, with carbon produced self-consistently via physical and chemical sputtering. In addition some time-independent calculations were done without impurities to further elucidate the physics. Good agreement was found with the experiment. In addition the role of flow reversal in the carbon contamination of the main plasma arising from divertor generated sources was clarified.

Keywords: ASDEX-Upgrade; B2-Eirene; Density limit; Edge modeling

1. Introduction

All tokamaks exhibit some form of density limit. Recently Borrass et al. [1] have argued that the maximum achievable density in a divertor tokamak is associated with complete divertor detachment, providing a limit for the midplane separatrix density. This can be mapped to a limit of the core density by introducing models for the pedestal (H-mode) [2] or density peaking (L-mode) and has been found to give good agreement with the empirically derived Greenwald limit [3].

In this paper the B2-Eirene scrape-off layer simulation package [4,5] is used to investigate this density limit in ASDEX-Upgrade L-mode conditions with a view to the impact of geometry and transverse SOL transport.

B2-Eirene couples two codes, the multi-fluid code B2 treating the plasma [6,7] and the Monte-Carlo code Eirene treating the neutrals [8]. B2-Eirene includes, in particular, the effects of volume recombination (radiative and three-body), impurity production by physical and chemical sputtering and the non-coronal radiation of impurities.

B2-Eirene was used to simulate density ramp discharges for L-mode hydrogen plasmas in both the new and old ASDEX-Upgrade divertor conditions (see Ref. [9] for details of the two divertor configurations). For these simulations a gas puff was used to raise the density (as in the experiment) and carbon physical and chemical sputtering acted as the source of impurities. (An earlier version of this work is described in Ref. [10].)

In Section 2 we discuss the use of the edge simulation code, B2-Eirene, to model the density limit, and in the following section compare results for the old and new divertor configurations. In Section 4 we discuss an additional facet that arose from our simulations – the impact of divertor generated impurities on the plasma outside the divertor.

2. Influence of transport on the density limit

Fig. 1 shows the operational diagram found from the experiment and Fig. 2 from the code when a gas puff was used to increase the density of an L-mode hydrogen plasma. Fig. 3 shows some experimental signals characterizing the experiment, and Fig. 4, the simulated signals from four B2-Eirene runs with different transport laws. Overall we find that the constant and Bohm cases give the best agreement.

3. Comparison of divertors I and II

We then compared the density limit in the new, more closed divertor. Fig. 5 indicates a somewhat lower den-

* Corresponding author. E-mail: dpc@ipp.mpg.de.

0022-3115/99/$ – see front matter
PII: S0022-3115(98)00882-4

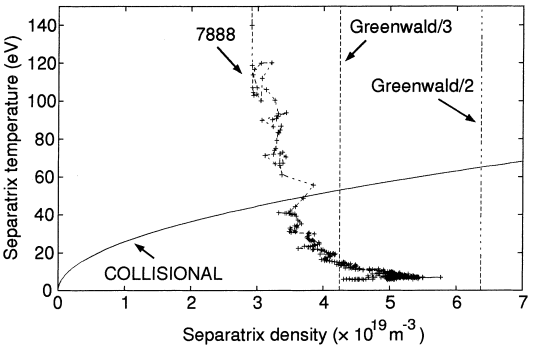

Fig. 1. Edge operational diagram showing the separatrix temperature plotted as a function of the separatrix electron density for a 5 MW L-mode shot in the divertor I configuration of ASDEX-Upgrade. Also indicated are a 'collisional' limit which gives a necessary condition for the existence of temperature gradients (and hence for MARFEs) and the Greenwald limit under the assumption that the line average density is equal to 1/2 or 1/3 the line average density. (The collisional limit compares $q_\psi R$ with $10^{17}(T^2/n_e)$ where q is the safety factor at the 95% flux surface, R the major radius in m, T the electron temperature in eV, and n_e the electron density in m^{-3}.)

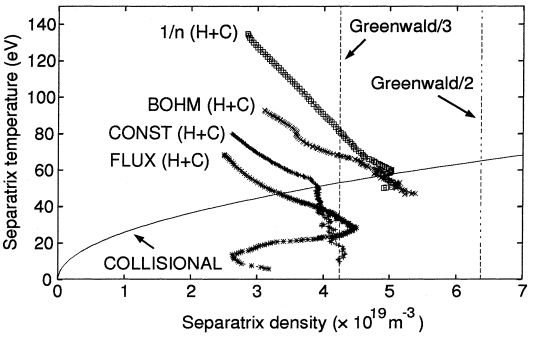

Fig. 2. Edge operational diagram for the divertor I density ramp simulations showing the separatrix temperature plotted as a function of the separatrix electron density for four different transport laws: spatially constant ('CONST'), Bohm ('BOHM'), flux scaled ('FLUX') and with the heat diffusivity proportional to a global $1/n$ ('1/n'). The other curves are described in Fig. 1.

sity limit for the new configuration, whereas the experiment seemed to indicate that the density limit is unchanged. In an effort to clarify this, pure H runs were performed for both configurations and the results are shown in Fig. 6. These were done as time stationary runs with no gas puff, and a "core" density boundary condition. In this case we see that there is no clear density limit in the sense that the code produces a "disruption" – what we do see is a rise in the volume recombination as a fraction of the total recombination, and a sinking of

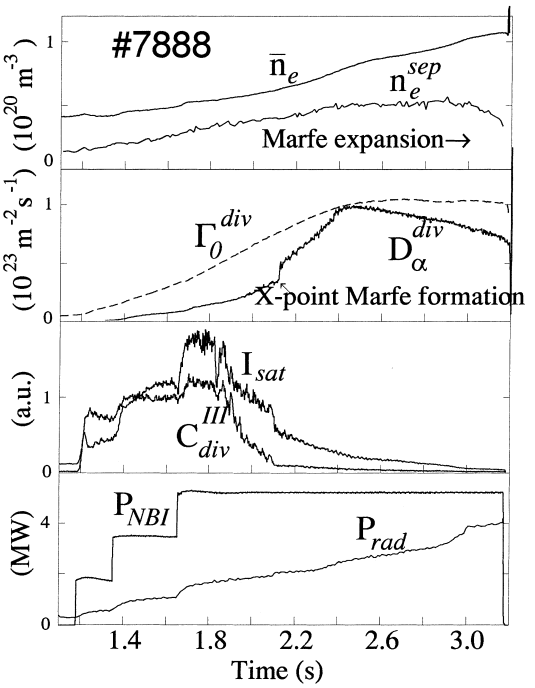

Fig. 3. Experimental traces for the 5 MW L-mode plasma performed with H in the divertor I ASDEX-Upgrade configuration. The quantities are, from top to bottom, the line averaged density, the separatrix density, the neutral flux density in the divertor, the H_α emission in the divertor, the ion saturation current, C-III line emission close to the target, the neutral beam input power and radiated power.

the upstream separatrix temperature. Both of these would lead to a density limit in the experiment and in the code if impurities were included.

Fig. 7 combines the density ramp simulation and discrete density simulation results for divertor II. The difference between the discrete density H+C 4 MW and ramp simulation results arises from the cooling in the divertor in the gas puff case (a much higher gas puff rate is used in the simulations than in the experiment to speed up the calculations). Divertor II is much more sensitive to this than divertor I because in divertor II the separatrix detaches earlier (in density) (as a result of the preferential scattering of recycling neutrals towards the divertor [9]). As can be seen in Figs. 8 and 9, the upstream conditions – the midplane separatrix electron temperature and density – are not much different for the gas puff and discrete density cases, but the target separatrix temperatures are distinctly lower for the gas puff case. This lower temperature causes an earlier (with increasing density) onset of volume recombination and complete detachment, and lowers the density limit for the gas puff case in contrast to the discrete density simulations.

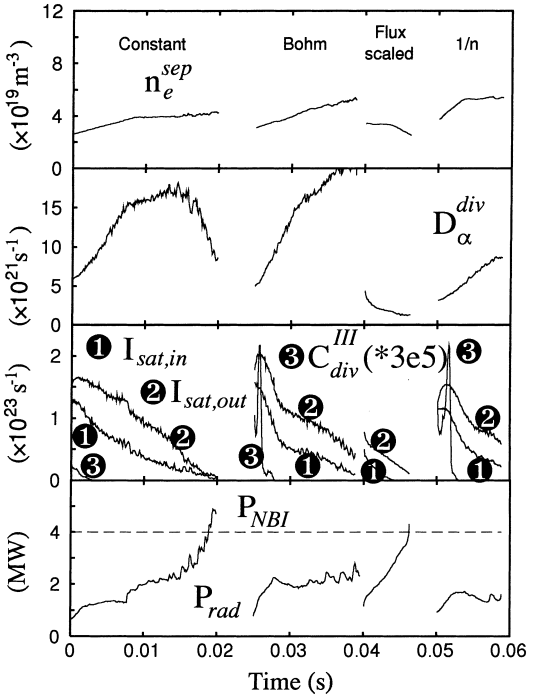

Fig. 4. B2-Eirene traces for the density ramp simulations. These were done with 4 MW of input power and four different transport coefficients were used: spatially constant, Bohm, flux scaled (i.e. constant expressed in toroidal flux) and the thermal diffusivity inversely proportional to density. From top to bottom, we have the electron density, the total H_α emission in the divertor, the ion saturation currents inboard and outboard, the C-III line emission, the input power and the radiated power.

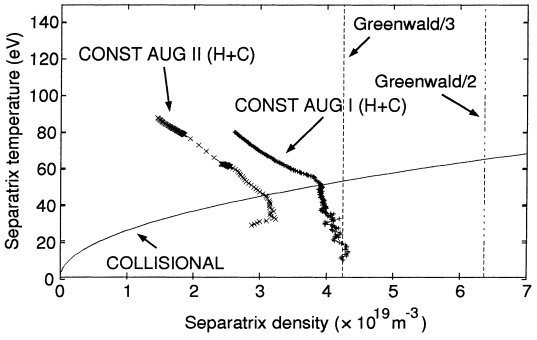

Fig. 5. Edge operational diagram comparing the density ramp simulations in divertor I and II, both with spatially constant transport coefficients. The other curves are described in Fig. 1.

4. C impurity accumulation

As a side-effect of the density limit analysis, we built up a database of a number of simulations, with and without C, over a range of densities and input powers.

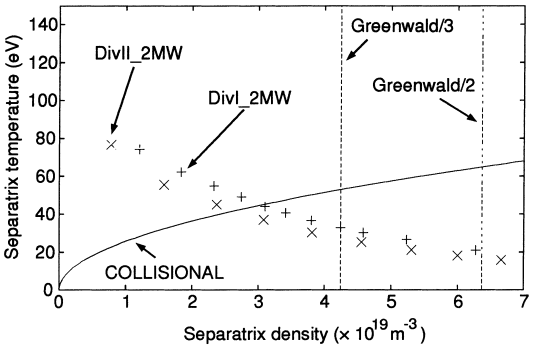

Fig. 6. Edge operational diagram for the discrete density simulations for divertor I and II. Both had 2 MW of input power, no impurities and the same, spatially constant, transport coefficients. The other curves are described in Fig. 1.

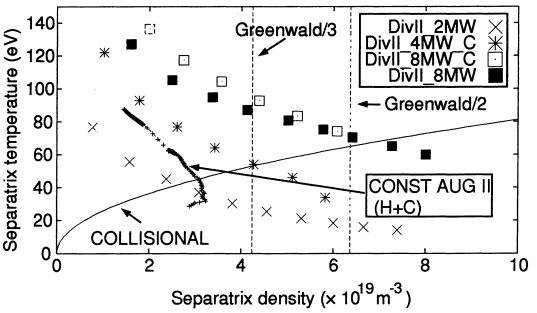

Fig. 7. Edge operational diagram combining different simulations for divertor II: the 4 MW power density ramp, 2 and 8 MW pure hydrogen discrete density simulations, and 4 and 8 MW H+C discrete density simulations. The other curves are described in Fig. 1.

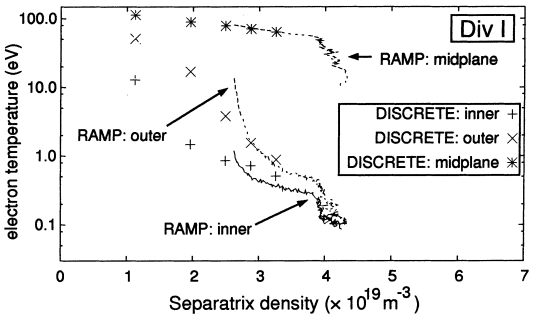

Fig. 8. Operational diagram for divertor I showing the separatrix inner strike point, outer strike point and midplane electron temperatures versus the midplane separatrix density for the 4 MW density ramp simulation and 4 MW discrete density H+C simulations.

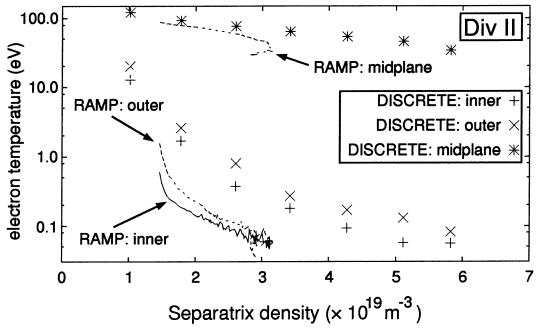

Fig. 9. Operational diagram for divertor II showing the separatrix inner strike point, outer strike point and midplane electron temperatures versus the midplane separatrix density for the 4 MW density ramp simulation and 4 MW discrete density H+C simulations.

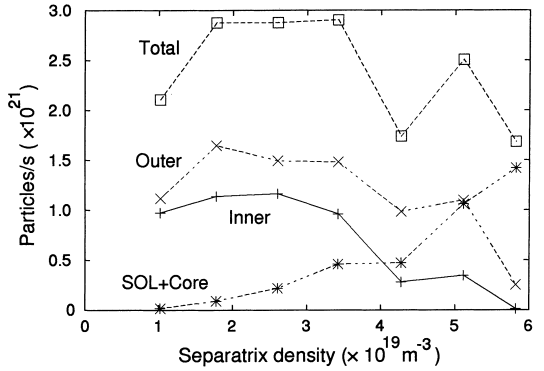

Fig. 10. The C source rates are plotted by region as a function of midplane separatrix density. The three regions are the inner divertor, the outer divertor and the rest of the plasma. These calculations were done for 4 MW L-mode hydrogen plasmas with physically and chemically sputtered carbon.

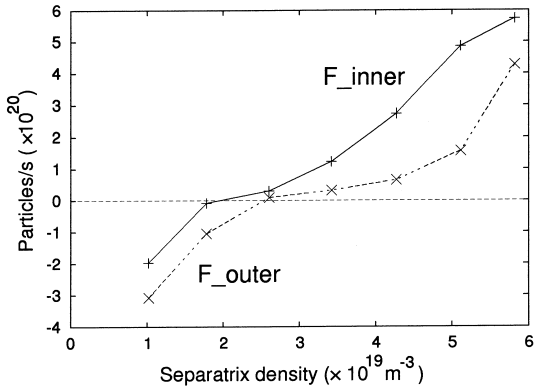

Fig. 11. The C fluxes arriving in the two divertors from the main plasma as a function of midplane separatrix density. Negative values imply that the divertor is acting as a source of C, positive that the divertor is a net sink of C.

One interesting aspect to emerge was the drop in upstream Z_{eff} once a critical density had been exceeded.

In Figs. 10 and 11 we see an initial rise of C impurity production with density in the two divertors corresponding to the increasing H flux (this is also associated with a fall in divertor temperatures, and hence an increasing role of chemical sputtering over physical sputtering), followed by a slow fall off as the density continues to rise. At the same time the C source outside the divertor region rises as the density increases, becoming the dominant source for the higher densities. We also see that at the lower densities the divertors act as a

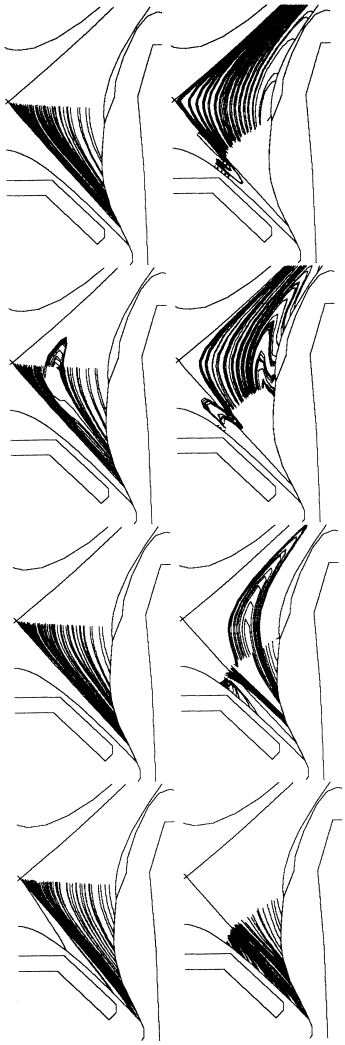

Fig. 12. From top to bottom, we have the H (left) and C (right) trajectories in their mean flow fields for "core" hydrogen densities of 1×10^{19}, 2×10^{19}, 3×10^{19} and 4×10^{19} (the corresponding midplane separatrix electron densities were 1.0209×10^{19}, 1.78046×10^{19}, 2.60546×10^{19} and 3.42116×10^{19}, respectively) m^{-3}.

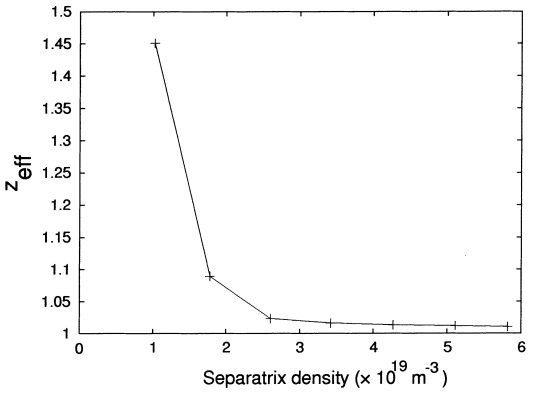

Fig. 13. Z_{eff} plotted as a function of midplane separatrix density.

source of C, but above a critical density they switch to being a net sink (with this transition occurring earlier for the inboard divertor).

To understand this behaviour we plot the trajectories of H and C test particles in their respective flow fields in Fig. 12 for the outer divertor.

For these cases we see strong streaming of H towards the divertor (with evidence of a small flow reversal zone for the 2×10^{19} case). For the three lower densities we see flow reversal for C, but for the 3×10^{19} case the particles return to the divertor.

Thus we can understand the leakage for the lower density cases in terms of this flow reversal for the impurity species.

The consequences of this are clearly seen in Fig. 13. For the cases where the divertor acts as a net source, the Z_{eff} is distinctly higher.

5. Conclusions

The density limit, at least in some circumstances, is associated with complete detachment and the onset of strong volume recombination in the divertor. The lack of a clear density limit in the H only simulations indicates that it is not only driven by hydrogen physics – there is a synergy between the complete detachment and MARFE formation.

The role of impurity flow reversal for the transport of impurities generated in the divertors into the main scrape-off layer is clarified: at low densities the divertors can act as a source of impurity contamination, while at higher densities the divertors act as a net sink of C, and the main source of main plasma impurity contamination arises in the main chamber.

References

[1] K. Borrass, R. Schneider, R. Farengo, Nucl. Fusion 37 (1997) 523.
[2] K. Borrass, J. Lingertat, R. Schneider, Contrib. Plasma Phys. 38 (1998) 130.
[3] M. Greenwald, J.L. Terry, S.M. Wolfe, S. Ejima, M.G. Bell et al., Nucl. Fusion 28 (1988) 2199.
[4] R. Schneider, D. Reiter, H.P. Zehrfeld, B. Braams, M. Baelmans et al., J. Nucl. Mater. 196–198 (1992) 810.
[5] D. Reiter, J. Nucl. Mater. 196–198 (1992) 80.
[6] B.J. Braams, Computational studies in tokamak equilibrium and transport, PhD thesis, Rijksuniversiteit, Utrecht, The Netherlands, 1986.
[7] B.J. Braams, Technical Report 68, Next European Torus, 1987.
[8] D. Reiter et al., J. Nucl. Mater. 220–222 (1995) 987, PSI 94 Mito.
[9] R. Schneider, H.-S. Bosch, D. Coster, J.C. Fuchs, J. Gafert et al., these Proceedings.
[10] D.P. Coster, H. Kastelewicz, R. Schneider, ASDEX-Upgrade Team, in: M. Schittenhelm, R. Bartiromo, F. Wagner (Eds.), Europhysics Conference Abstract, Proceedings of the 24th EPS Conference on Controlled Fusion and Plasma Physics, Berchtesgaden, 1997, vol. 21A, Part IV, Petit-Lancy, EPS, 1997, pp. 1437–1440.